J. Fluid Mech. (1995), *vol.* 297, *pp.* 193–214

Pressure-impulse theory for liquid impact problems

By MARK J. COOKER† AND D. H. PEREGRINE
School of Mathematics, University of Bristol, Bristol BS8 1TW, UK

(Received 16 September 1991 and in revised form 10 April 1995)

A mathematical model is presented for the high pressures and sudden velocity changes which may occur in the impact between a region of incompressible liquid and either a solid surface or a second liquid region. The theory rests upon the well-known idea of pressure impulse, for the sudden initiation of fluid motion in incompressible fluids. We consider the impulsive pressure field which occurs when a moving fluid region collides with a fixed target, such as when an ocean wave strikes a sea wall. The boundary conditions are given for modelling liquid–solid and liquid–liquid impact problems. For a given fluid domain, and a given velocity field just before impact, the theory gives information on the peak pressure distribution, and the velocity after impact. Solutions for problems in simple domains are presented, which give insight into the peak pressures exerted by a wave breaking against a sea wall, and a wave impacting in a confined space. An example of liquid–liquid impact is also examined. Results of particular interest include a relative insensitivity to the shape of the incident wave, and an increased pressure impulse when impact occurs in a confined space. The theory predicts that energy is lost from the bulk fluid motion and we suggest that this energy can be transferred to a thin jet of liquid which is projected away from the impact region.

1. Introduction

When a moving body of liquid strikes a target such as a rigid surface or another body of liquid, large and short-lived pressures are generated. The work described here was motivated by study of the impact of water waves against vertical walls, a frequent occurrence where coastal structures face the open sea. This application dominates our discussion so we clarify some terminology. Coastal engineers refer to 'shock pressures' when describing the large brief pressures of wave impact, but there is no decisive evidence that water wave impact is associated with shock waves of compression in the fluid. So instead we use 'impact pressure' as the generic term. Further, 'hydrostatic pressure' is used as usual to denote the quantity $\rho g Y$ where Y is the instantaneous depth below the free surface. The pressure $\rho g H$, where H is the height of the top of the wave above the bed, is a convenient hydrostatic reference pressure. The 'impact zone' is that part of a surface which is struck by the moving fluid. The term 'peak pressure' means the greatest pressure recorded at a given position as a function of time during impact.

There is a long history of observations on the movement of rocks and structures by coastal waves (e.g. see Stevenson 1886), and of experiments to measure the pressures induced by waves breaking against vertical walls at normal incidence. Reliable pressure recordings were first achieved with electrical recording equipment by de Rouville, Besson & Petry (1938) and Bagnold (1939). They and succeeding experimenters, such

† Present address: School of Mathematics, University of East Anglia, Norwich NR4 7TJ, UK.

as Denny (1951), Nagai (1960), Richert (1968) and Kirkgöz (1982) report a wide scatter ($\pm 50\%$) in their measurements of peak pressure at the wall. More recently probability distributions of impact pressures have been reported by Fürhböter (1986), Witte (1988) and Kirkgöz (1991) from nominally periodic waves. We are here concerned with the most extreme pressures generated by breaking waves.

The size and duration of water-wave impact pressure are relatively well documented. Blackmore & Hewson (1984) report and review field measurements of sea wave impact pressures. For a wave with a height of about 1 m the maximum peak pressure can be as great as 10^5 N m^{-2} (10 tonnes force m^{-2} $\approx$ 10 m head of water). The pressure rises and falls in a time of the order 1 ms. Figure 1 is a sketch of a typical record of pressure as a function of time, at a point on the wall. In careful experiments laboratory waves produce impact pressures (relative to hydrostatic) which are much greater than those found in the field. Bagnold (1939), using 30 cm high waves, reported impact pressures thirty times the hydrostatic pressure.

There have been several theories of wave impact pressure. Bagnold (1939) proposes a model involving the compression of air between the vertical breaking wave face and the wall. Weggel & Maxwell (1970), and Partenscky & Tounsi (1989) model impact pressures by solving the wave equation in a compressible fluid with pressure sources at the wall. Among coastal engineers the work of Goda (1985) is often used in design.

The impact of other liquid bodies such as drops of water has had more attention. Many of these studies have been for high-speed impact in which significant shock waves are generated and which play a dominant role in the flow for much of the initial stages of impact. For example see the analytic studies of Lesser (1981), and Korobkin (1992, 1994*a*, *b*) and the experimental observations of Lesser & Field (1983). The impact of an incompressible droplet on to a rigid plane was studied analytically by Savic & Boult (1957) and numerically by Hwang & Hammitt (1977). In addition there has been a sequence of papers on the self-similar flows generated by a fluid wedge meeting a rigid plane: see Cumberbatch (1960) and Johnstone & Mackie (1973). The water entry of a solid wedge into liquid can also be modelled by a self-similar flow: see Cointe (1989) and Howison, Ockenden & Wilson (1991). The water-entry problem is reviewed by Korobkin & Pukhnachov (1988).

Bagnold (1939) observed experimentally that under fixed wave conditions (at a given point on the wall) the pressure impulse is approximately constant, even though the peak pressure changes unpredictably between apparently identical wave impacts. Pressure impulse P is defined by

$$P(x) = \int_{t_b}^{t_a} p(x, t)\, \mathrm{d}t, \tag{1.1}$$

where t_b and t_a are the times immediately before and after impact, respectively. The subscript conventions b for 'before impact' and a for 'after impact' are used throughout. Even though the peak pressure varies unpredictably, the pressure impulse is relatively well behaved. This is partly confirmed by the measurements of Richert (1968), and suggests that the pressure impulse is a better physical quantity to model than the peak pressure.

Lamb (1932, §11) shows how the velocity potential of an irrotational flow can be interpreted as that pressure impulse which can instantaneously accelerate the fluid from rest to its present velocity. Pressure impulse is used to model the flows instantaneously induced from rest by, for example, the impact of a rigid body hitting the surface of still water. See Wagner (1932), Batchelor (1973, §6.10), the general treatment of Sedov (1965), and the review of Korobkin & Pukhnachov (1988). Cointe

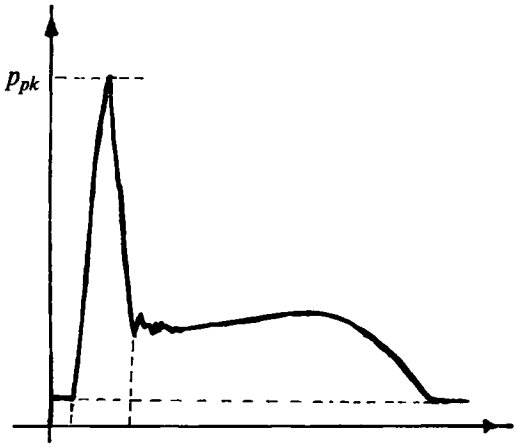

FIGURE 1. Sketch of the pressure as a function of time at a point on a sea wall undergoing wave impact.

(1989), Cointe & Armand (1987), and Howison *et al.* (1991) all solve problems of rigid-body impact on still water. Their outer solutions for the velocity potential of the induced irrotational flow can be interpreted as fields of pressure impulse.

When a body strikes a fluid at rest a transient pressure field occurs throughout the field. The pressure rises and falls in the short time, Δt, and the gradient of the pressure field accelerates the fluid into motion. In this paper we turn this idea around, and consider the pressure impulse in a *moving* liquid domain which collides with a fixed structure. The impulsive pressure gradients accelerate the fluid from an incident velocity to a new velocity field. Although liquid-on-solid impacts have been much studied for high-speed collision, and liquid–liquid impacts are briefly discussed in Howison *et al.* (1991) there seems to be little previous investigation of the simple pressure-impulse model in this context, except for an exercise in Milne-Thomson (1968).

In this paper the impact speed is taken to be much less than the speed of sound in the liquid, so that incompressible fluid is a reasonable model and impulsive pressures in the domain of interest occur within the same short time interval, $[t_b, t_a]$. This, and the neglect of many details of motion in the neighbourhood of the impact zone, are the major assumptions of pressure-impulse theory. They are discussed further in the concluding section.

The mathematical formulation of the problem is briefly presented in §2. The major part of the paper is the presentation of some solutions for simple geometries in §3. The sudden change in velocity that occurs on impact is next presented together with some comments on splashing. Energy is lost in the pressure impulse model, as demonstrated in §5, and this is discussed within the context of waves meeting a wall.

2. Mathematical formulation

The concept of pressure impulse, or impulsive pressure, is well-known (Lamb 1932, §11, Batchelor 1967, §6.10). The change in velocity during the impulsive event is supposed to take place over such a short time that the nonlinear convective terms in the equation of motion are negligible compared with the time derivative, giving

$$\frac{\partial \boldsymbol{u}}{\partial t} = -\frac{1}{\rho}\nabla p. \tag{2.1}$$

Viscosity and surface tension are negligible in all applications we have considered. Although compressibility may be important for a brief moment, even for impact velocities well below the speed of sound, it is neglected here. It is easy to see that next to the impact zone there is a small region where nonlinear terms are not negligible, e.g. see Howison *et al.*'s (1991) treatment of water entry; however, the pressure-impulse approach gives a good 'outer' approximation (see also the discussion of energy loss in §5).

We integrate equation (2.1) with respect to time through the impact interval, $[t_b, t_a]$, and use definition (1.1) for the pressure impulse P, to arrive at

$$\boldsymbol{u}_a - \boldsymbol{u}_b = -\frac{1}{\rho}\nabla P, \tag{2.2}$$

where $\nabla \cdot \boldsymbol{u}_b$ and $\nabla \cdot \boldsymbol{u}_a$ both vanish. Taking the divergence of (2.2), we find that the pressure impulse satisfies Laplace's equation

$$\nabla^2 P = 0. \tag{2.3}$$

Consideration of the curl of (2.1) and (2.2) shows that the pressure impulse does not change the vorticity of the flow.

The boundary conditions to be applied to Laplace's equation are readily found to be as follows.

(*a*) At a free surface, where the pressure is constant and taken to be a zero reference pressure: $P = 0$.

(*b*) At a stationary rigid boundary, in contact with the liquid before and after the impulse, the normal velocity is unchanged so that

$$\partial P/\partial n = 0. \tag{2.4}$$

(*c*) Where liquid meets a solid boundary during impact the change in normal velocity gives the normal derivative of pressure impulse. For the simplest case of a stationary rigid boundary

$$u_{nb} = \frac{1}{\rho}\frac{\partial P}{\partial n}, \tag{2.5}$$

where u_{nb} is the normal component of the approach velocity of the liquid.

Conditions (*b*) and (*c*) are easily altered to account for moving rigid boundaries including the case where the impact causes a rigid body to move (e.g. see Cooker & Peregrine 1992).

(*d*) When liquid meets liquid two boundary conditions are needed on the common interface. One is that the pressure impulse is continuous:

$$P_1 = P_2. \tag{2.6}$$

Consideration of the change in velocity on each side of the interface gives

$$u_{1nb} - u_{2nb} = \frac{1}{\rho_1}\frac{\partial P_1}{\partial n} - \frac{1}{\rho_2}\frac{\partial P_2}{\partial n}, \tag{2.7}$$

where subscript n denotes the component normal to the boundary and subscript b denotes the liquid velocities immediately before the impact.

In all the above cases, an inelastic impact is assumed.

3. Solutions for waves and jets in simple geometries

A number of simple, idealized examples of liquid impact are given below. Note in particular the following.

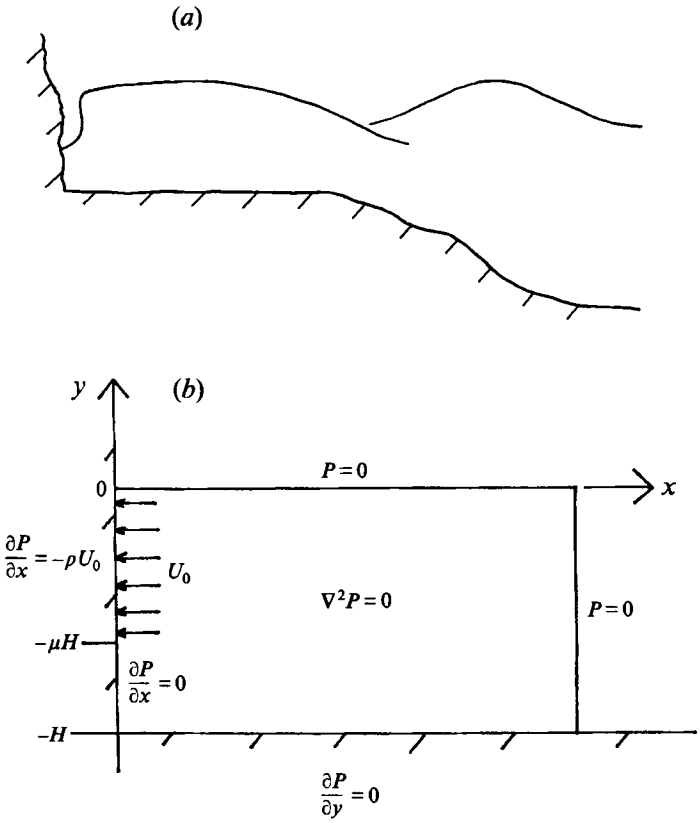

FIGURE 2. (*a*) Sketch of a coastal wave impact. (*b*) The impact of a rectangle of fluid on a vertical wall at $x = 0$. The impact zone stretches from the top free surface, part-way down the wall, occupying a fraction μ of water height, H. The back of the wave at $x = b$ is a free surface with $P = 0$.

(i) Pressure-impulse fields close to the impact region depend on the distribution of the normal component of impact velocity over that region. Here it is taken to be uniform for simplicity but there is no difficulty in choosing other velocity distributions in the examples that follow.

(ii) Any contour C of pressure impulse can be used as an alternative free boundary, since subtraction of the value of pressure impulse on C from $P(x, y, t)$ gives another pressure impulse field which is zero on C.

(iii) As is indicated by pressure-impulse fields and comment (ii) above, the pressure impulse acting on the rigid boundaries is only weakly dependent on the shape of the free boundary. This is also illustrated in the results for rectangular impacting shapes, and implies that simplified representations of the impacting liquid's shape can be of value in practical circumstances.

3.1. *Impact of an idealized wave on a vertical wall*

A realistic wave impact is sketched in figure 2(*a*). Figure 2(*b*) shows a two-dimensional boundary-value problem for an idealized water wave meeting a rigid vertical wall. The fluid domain has been idealized to a rectangle with free surfaces at the upper and right-hand edges ($y = 0$, $x = b$). Fluid stays in contact with the bed and the lower part of the wall, and the wave face impacts on the upper part of the wall. The distance from the

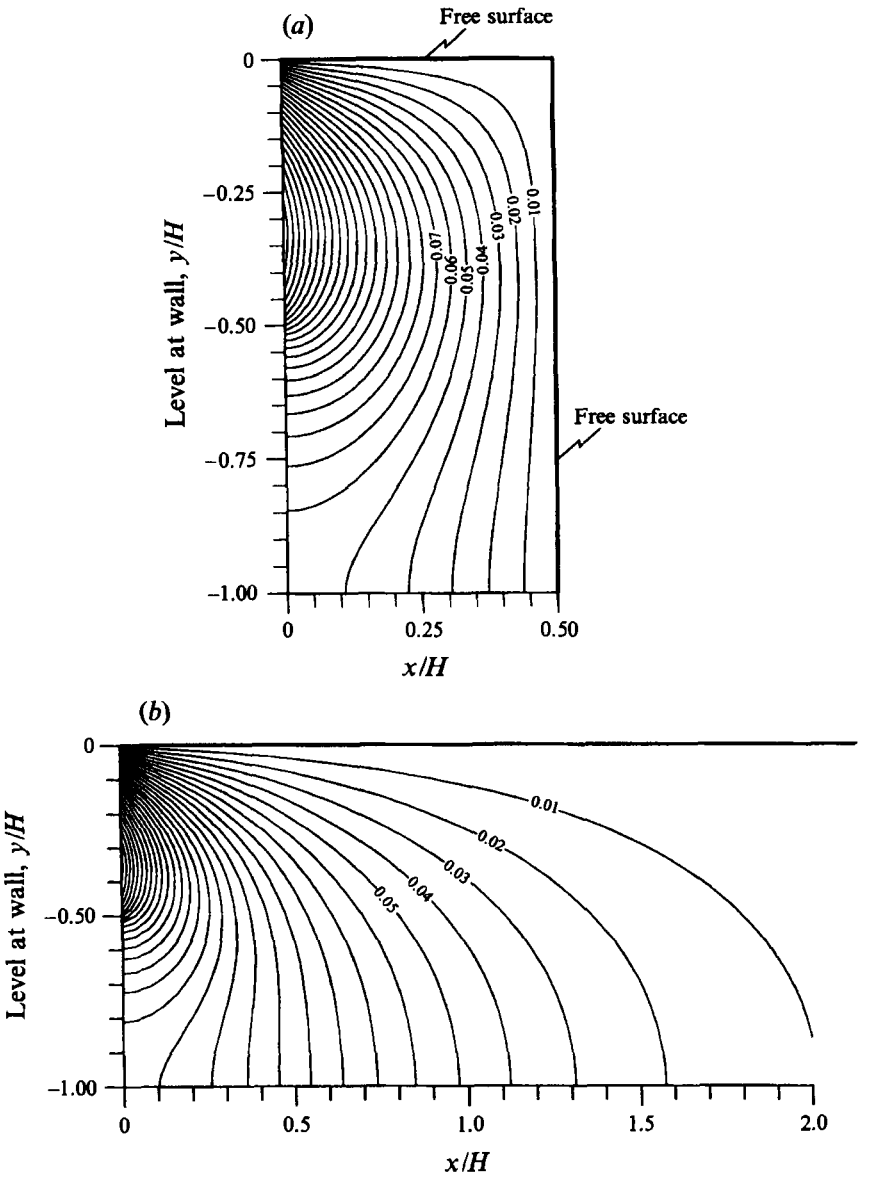

FIGURE 3. Contours of pressure impulse for the arrangement in figure 2(*b*) for $H = \rho = U_0 = 1$, $\mu = 0.5$. Contour interval $= 0.01(\rho U_0 H)$. (*a*) $b = 0.5$; the maximum value of P is $0.248(\rho U_0 H)$, and occurs at the wall, $x = 0$. (*b*) $b = \infty$; the maximum pressure impulse is $0.293(\rho U_0 H)$.

bed to the wave crest is H, and the wave strikes a fraction μ of this height. We model the normal component of impact velocity as a constant: $U_0 > 0$ in the impact zone $x = 0$, $-\mu H \leqslant y \leqslant 0$, though a general distribution of impact speed $u_{nb}(y)$ can be easily accounted for by the following method. The boundary conditions are as shown in figure 2(*b*). The problem is solved using separation of variables in Laplace's equation, and Fourier analysis, giving

$$P(x,y) = \rho H \sum_{n=1}^{\infty} a_n \sin(\lambda_n y/H) \frac{\sinh[\lambda_n(b-x)/H]}{\cosh(\lambda_n b/H)} \tag{3.1}$$

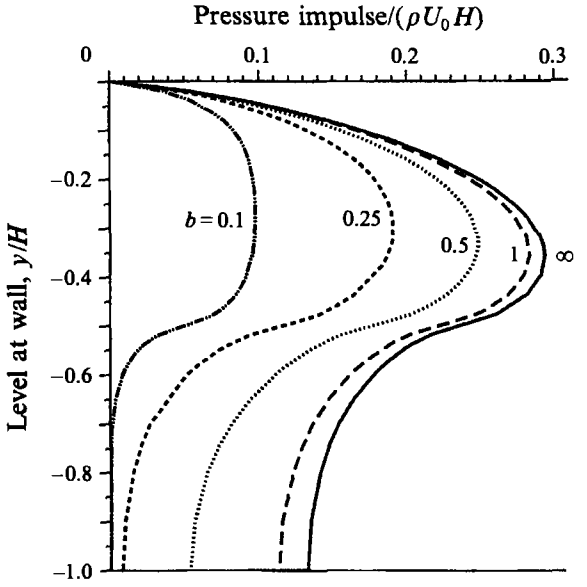

FIGURE 4. The pressure impulse at the wall as a function of position y/H below the surface for the configuration of figure 2(b); $\mu = 0.5$. Each curve is for a different value of domain length, b.

for $-H \leqslant y \leqslant 0$, and $0 \leqslant x \leqslant b$ where $\lambda_n = (n-\frac{1}{2})\pi$, and the constants a_n are

$$a_n = 2U_0 \frac{\cos \mu\lambda_n - 1}{\lambda_n^2}.$$

For $b \gg H$, the solution can also be expressed as an integral from which some explicit results may be obtained (see the Appendix, equation (A 6)) but the series in (3.1) is generally more convenient for computing P. However, if the velocity change is required care should be taken in regions where the Fourier series converges very slowly.

The pressure-impulse distribution for two contrasting examples, each with $\mu = 0.5$, are shown in figures 3(a) and 3(b). Although the second example has a much smaller volume of liquid the pressure-impulse distributions near the impact wall are very similar: the difference in pressure impulse is only $0.06\,\rho U_0 H$ to $0.08\,\rho U_0 H$ smaller. The effect of reducing the rectangle size further is shown in figure 4, where plots of pressure impulse down the impact wall are shown for various b/H. Except for relatively thin layers of liquid, $b/H \leqslant 0.25$, the profiles of pressure impulse are similar, showing significant values right down to the bed.

For modelling water waves values of $b/H \geqslant 1$ are probably more appropriate, and these are well represented by the case $b/H \to \infty$. The pressure-impulse profiles on the impact wall for a range of values of μ are shown in figure 5 for $b/H = \infty$. All examples show significant values of pressure impulse below the impact zone. The case $\mu = 1$ can, by reflection in the bed, be taken to represent the pressure impulse due to impact by a two-dimensional jet with a blunt front face. The maximum value of P in this case is $0.742\,\rho U_0 H$.

Figure 6 shows the total impulse on the wall as a function of μ for various values of b. The solution curve for $b = 1$ is a fair approximation of that for the semi-infinite rectangle ($b = \infty$). This implies that the momentum lost from a wave during impact comes from that part of the liquid domain which is near the wall. Far from the wall little of the horizontal component of momentum is lost, and the geometry of the fluid

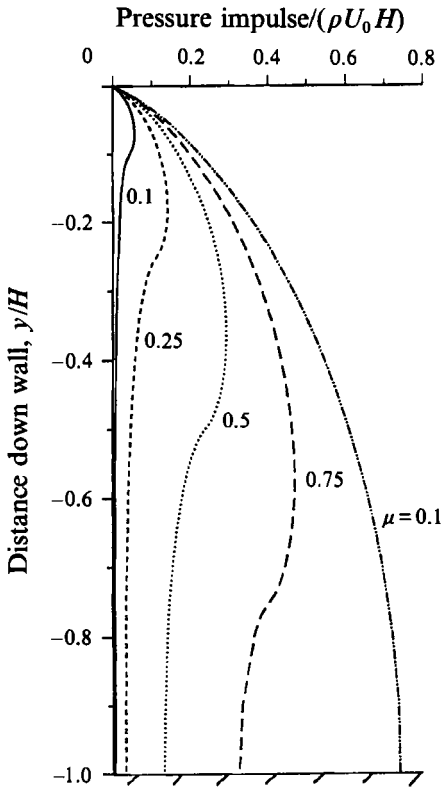

FIGURE 5. As figure 4: pressure impulses at the wall for $b = \infty$. Each curve is for a different value of μ.

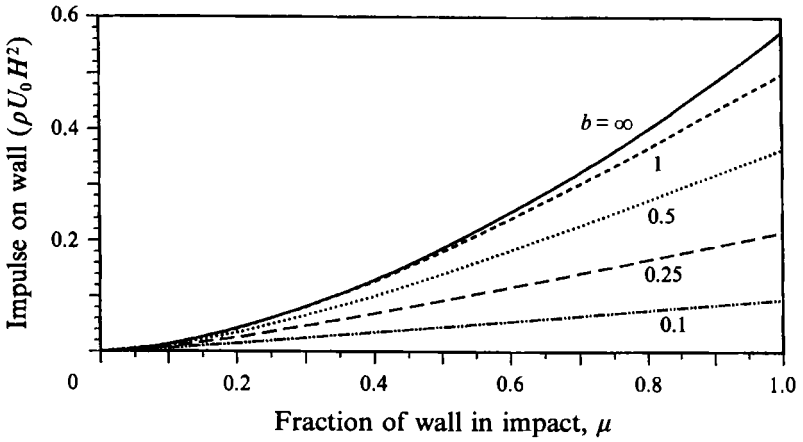

FIGURE 6. The total impulse as a function of μ, for the configuration of figure 2(*b*). Each curve is for a different value of the domain length, b.

domain more than a distance H from the wall has little effect on the total impulse on the wall. We make this idea more precise by introducing the momentum length, L_m, defined by

$$L_m = \frac{1}{\rho U_0 \mu H} \int_{-H}^{0} P(0, y)\, \mathrm{d}y. \tag{3.2}$$

For the open-backed rectangle of figure 2(*b*)

$$L_m = 2H \sum_{n=1}^{\infty} \frac{1-\cos \mu\lambda_n}{\mu\lambda_n^3} \tanh(\lambda_n b/H). \tag{3.3}$$

As the width of fluid b/H tends to zero the momentum length is asymptotically equal to b. The maximum value of L_m is $0.542H$ for $\mu = 1$ and $b/H = \infty$.

3.2. *Impact of deep water waves*

For waves which occupy a quarter-space, in deep water, we have $b = \infty$, and $H = \infty$, and a Fourier series approach is inappropriate. Roberts (1987) has solved the almost identical boundary-value problem for the impulsive motion of a vertical wavemaker. Let the impact zone have height d, let $z = x + \mathrm{i}y$ describe position in the complex plane and let the complex function $\mathscr{P}(z)$ be such that $\mathrm{Re}\{\mathscr{P}\} = P$, then

$$\frac{\mathrm{d}\mathscr{P}}{\mathrm{d}z} = \frac{\partial P}{\partial x} - \mathrm{i}\frac{\partial P}{\partial y} = -\frac{\mathrm{i}\rho U_0}{\pi} \log(1 + d^2/z^2)$$

and so

$$P = -\mathrm{Im}\frac{\rho U_0}{\pi}[(z+\mathrm{i}d)\log(z+\mathrm{i}d) + (z-\mathrm{i}d)\log(z-\mathrm{i}d) - 2z\log z]. \tag{3.4}$$

On the wall $z = \mathrm{i}y$ and the pressure-impulse distribution is

$$P(0,y) = -\frac{\rho U_0}{\pi}[y\log|1-d^2/y^2| + d\log|(d+y)/(d-y)|]. \tag{3.5}$$

At great depth the impulse at the wall is asymptotically

$$P(0,y) \sim -\rho U_0 d^2/(\pi y) \quad \text{as} \quad y \to -\infty.$$

3.3. *Impact in a container*

Somewhat higher pressure impulses than those of §3.1 are found in confined spaces. If $x = b$ is a stationary rigid surface, corresponding to wave impact on the inside of an open-topped tank, the series solution is now

$$P(x,y) = 2\rho U_0 H \sum_{n-1}^{\infty} \frac{\cos \mu\lambda_n - 1}{\lambda_n^2} \sin[\lambda_n y/H] \frac{\cosh[\lambda_n(b-x)/H]}{\sinh[\lambda_n b/H]}. \tag{3.6}$$

The corresponding momentum length is

$$L_m = 2H \sum_{n-1}^{\infty} \frac{1-\cos \mu\lambda_n}{\mu\lambda_n^3} \coth[\lambda_n b/H]. \tag{3.7}$$

Figure 7 shows the pressure-impulse distribution, at $x = 0$, for several values of b. Note that the maximum value of P increases as the tank length is reduced. This shows that waves confined in containers can exert much greater impact pressures than when the waves are unconfined. This is apparent in the momentum length given by (3.7), which is greater than that for an open-backed wave (equation (3.3)). The distribution of pressure impulse in the fluid is shown in figure 8 for $\mu = 0.5$, $b = 1$, enabling comparison with figure 3(*b*).

In yet more confined spaces, such as in a wave-cut notch in a cliff, or in a deep narrow masonry joint, we may expect yet higher pressure impulses. However, the role

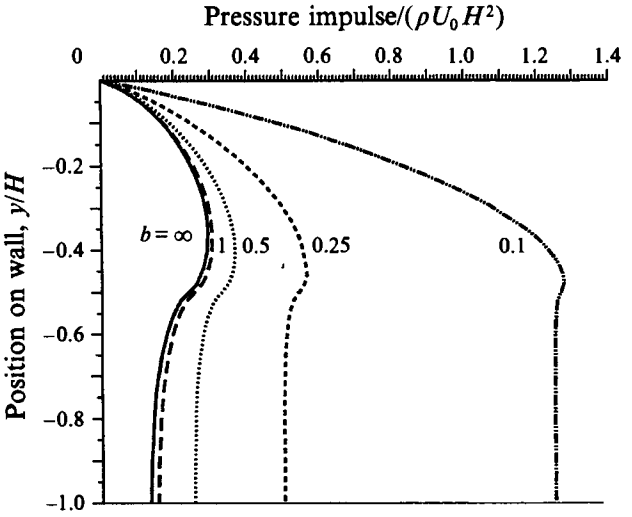

FIGURE 7. The pressure impulse at the wall for wave impact within a container; $\mu = 0.5$. Note that the maximum impulse increases rapidly as b decreases, showing that the more confined the container, the greater the impulse on the wall.

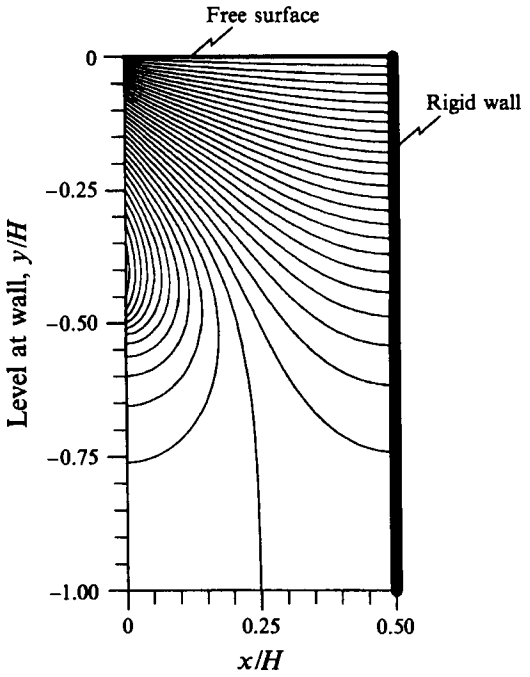

FIGURE 8. Contours of pressure impulse for wave impact within a container. $H = \rho = U_0 = 1, \mu = 0.5$. Contour interval = 0.01. The maximum value of P is $0.367\rho U_0 H$, which is 50% greater than in figure 3(*a*).

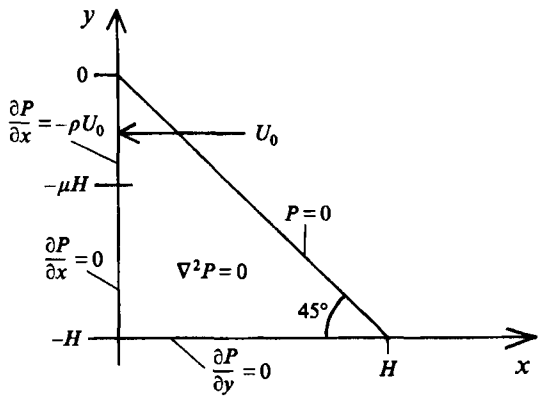

FIGURE 9. The boundary-value problem for the impact of a wave, with a 45° triangular section, on a vertical wall. μ is the fraction of the wall struck.

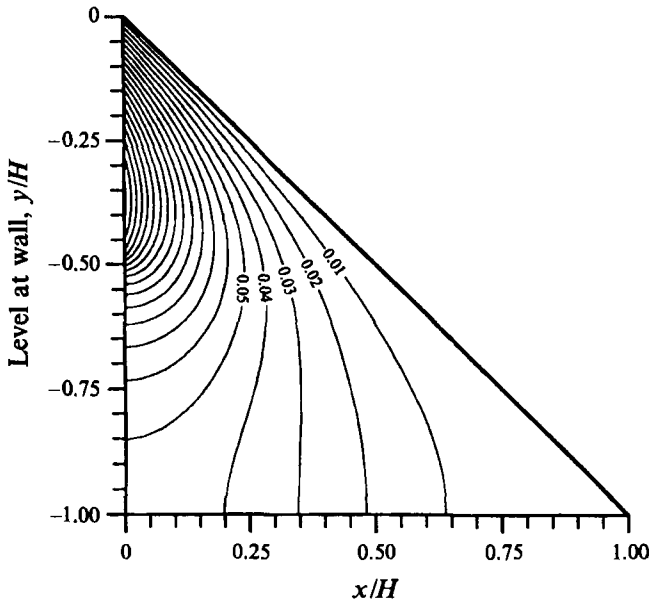

FIGURE 10. Pressure impulse contours for $\mu = 0.5$, $H = \rho = U_0 = 1$, for the configuration of figure 9. The maximum of P is $0.194(\rho U_0 H)$.

of air trapped in such spaces by impacting water may well lessen the pressure predicted by our simple analysis. On the other hand a liquid-filled crack may convey high impulsive pressures deep inside a structure.

3.4. *A triangular wave*

An isosceles triangular wave as sketched in figure 9 shows similar results. The meaning of the terms impact speed, U_0, and the impact zone height μH are the same as for the rectangles discussed above. To solve Laplace's equation with the given boundary conditions it is easier to consider the equivalent problem in a square with antisymmetry about its diagonal (this ensures that $P = 0$ on the free surface). The

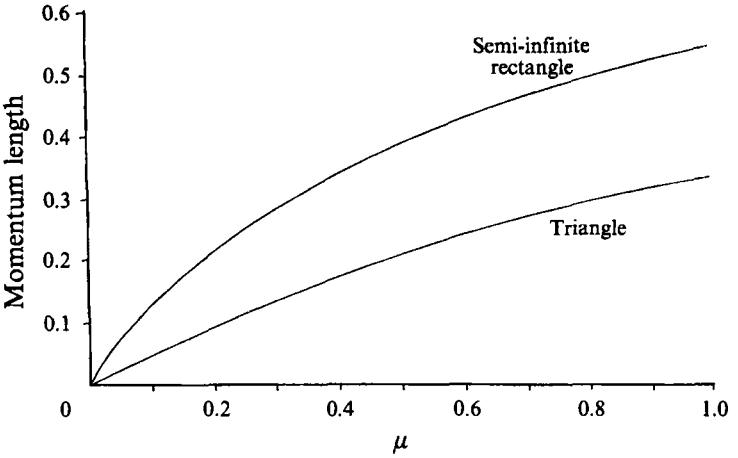

FIGURE 11. The momentum length as a function of μ for a semi-infinite rectangular wave and for a triangular wave. Although the triangle is much smaller it exerts about half the pressure impulse of the semi-infinite wave except when μ is small.

solution is not as straightforward as for the rectangular wave, but is easily put in a similar form by first introducing quadratic terms, giving

$$\frac{P(x,y;\mu)}{\rho U_0 H} = \tfrac{1}{2}\mu[(1+y/H)^2-(1-x/H)^2]$$

$$+\frac{2}{\pi^2}\sum_{n=1}^{\infty}\frac{\sin(n\pi\mu)}{n^2\sinh n\pi}\left[\cos\frac{n\pi x}{H}\cosh n\pi(1+y/H)-\cos\frac{n\pi y}{H}\cosh n\pi(1-x/H)\right]. \quad (3.8)$$

Figure 10 shows the contours of pressure impulse in the triangle for $\mu = 0.5$. The total impulse on the wall is

$$I = \rho U_0 H^2\left[\tfrac{1}{3}\mu-\frac{2}{\pi^2}\sum_{n=1}^{\infty}\frac{1}{n^3}\sin n\pi\mu\right] \quad (3.9)$$

which reduces to an Euler polynomial (Jolley 1961, series no 525):

$$I = \tfrac{1}{2}\rho U_0 H^2\mu^2(1-\tfrac{1}{3}\mu). \quad (3.10)$$

The maximum value of the impulse is $\frac{1}{3}\rho U_0 H^2$, which occurs when $\mu = 1$. The momentum length, L_m, of the triangle is

$$L_m = \tfrac{1}{2}H\mu(1-\tfrac{1}{3}\mu). \quad (3.11)$$

The function $L_m(\mu)$ is shown in figure 11 which permits comparison with the values for the semi-infinite rectangular wave. The triangle is of only finite extent but it exerts about one half of the impulse of the bigger wave (except when μ is small). From equation (3.11) the momentum length is at most one third of H.

3.5. *An axisymmetric jet-like impact*

A blunt circular cylindrical jet, radius a, of finite length, d, impacting on a rigid plane with uniform velocity U_0 is modelled as a semi-infinite rectilinear circular cylinder $0 < r < a$, $0 < z < d$. The pressure-impulse problem has the Fourier–Bessel series solution

$$P(r,z) = \sum_{n=1}^{\infty}\frac{2\rho U_0 J_0(k_n r)\sinh[k_n(d-z)]}{k_n^2 a J_1(k_n a)\cosh k_n d} \quad (3.12)$$

in which $k_n a = j_{0,n}$ the nth zero of the zeroth-order Bessel function J_0.

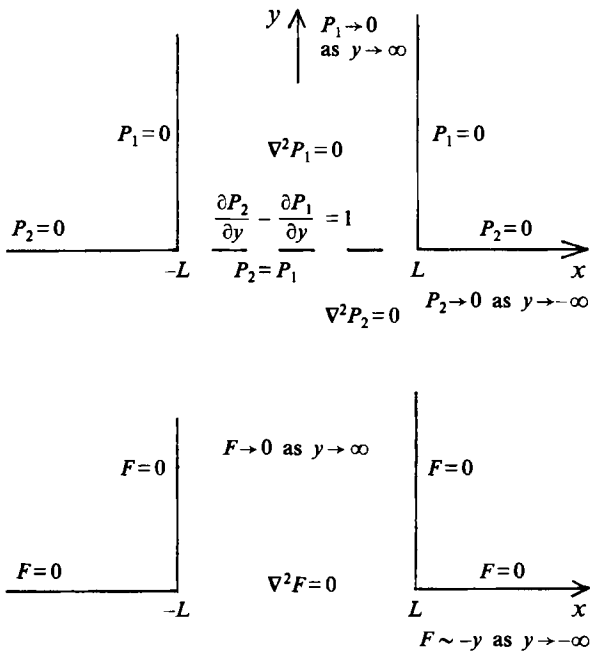

FIGURE 12. Impact of a two-dimensional jet on a lower half-plane of the same fluid. $U_0 = \rho = 1$.

The pressure-impulse maximum lies at $r = 0$, $z = 0$ and has the value, when $d = \infty$,

$$P(0,0) = \rho U_0 a^{-1} \sum_{n=1}^{\infty} \frac{2}{k_n^2 J_1(k_n a)} \tag{3.13}$$

which is approximately $0.535 \rho U_0 a$. The impact produces an impulse, $I \approx 0.323 \rho U_0 \pi a^3$, on the plane $z = 0$, giving a momentum length of $L_m \approx 0.323a$. In view of this fact, we may expect this solution to be a fair approximation for other (axisymmetric) regions of fluid which are of finite height d, where $d \gg 0.32a$.

3.6. *The impact of a water sheet on still water*

Figure 12 shows the pressure-impulse problem for the impact of a rectangular sheet of half-width L, meeting a half-plane of fluid at rest, with a closing speed U_0. Boundary conditions are shown and correspond to those in (2.6) and (2.7). The two fluids have the same density. In the following, subscripts 1 and 2 refer to the sheet (region R_1) and to the target liquid (region R_2) respectively. This mixed boundary-value problem is awkward in that P is unknown and the normal derivative of P is discontinuous at the impact zone. However, this particular problem can be solved by first defining in the region $y < 0$ the harmonic function

$$F(x,y) = P_2(x,y) - \rho U_0 y. \tag{3.14}$$

At the impact zone the boundary conditions become $P_1 = F$, and $\partial P_1/\partial y = \partial F/\partial y$. Since P_1 and F are harmonic we can infer that all the partial derivatives of P_1 equal the corresponding derivatives of F in the impact zone. Therefore F is a smooth continuation of P_1 into the lower half-plane. So we need not distinguish between the

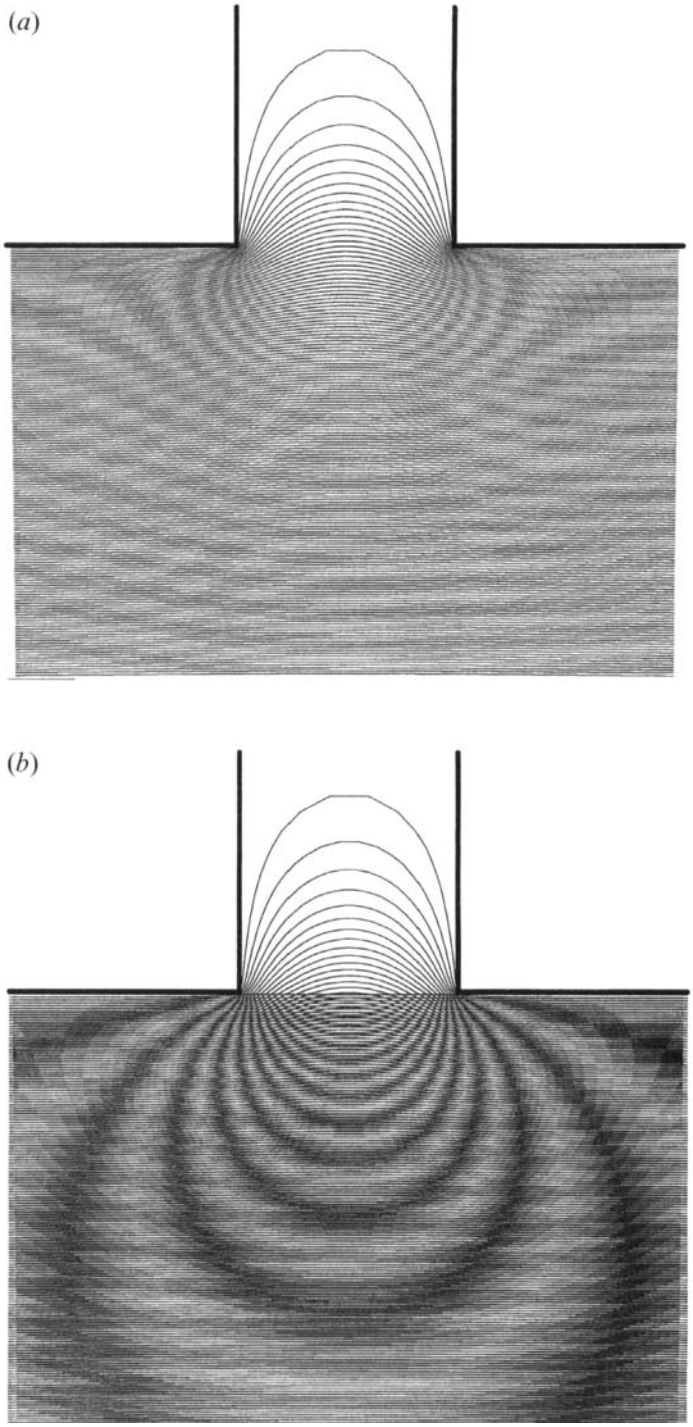

FIGURE 13. (*a*) The uniform steady flow past a wall containing a slot. The streamlines are the contours of $F(x, y)$. $F = P_1$ in the jet and $F = P_2 - \rho U_0 y$ in the lower half-plane. (*b*) The contours in the jet are of P_1. The dark and light bands in the lower half-plane are contours of P_2. The contour interval is $0.0267(\rho U_0 L)$. The maximum pressure impulse is $0.427(\rho U_0 L)$, at the centre of the impact zone.

two functions, and we denote them by $F(x, y)$, a continuously differentiable function in $R_1 \cup R_2$. The impact zone need no longer be treated as a boundary, because on ∂I, F is continuous with continuous first and second derivatives there. On the free surface $F = 0$, and at infinity we have the conditions

$$F \sim -\rho U_0 y \quad \text{as} \quad y \to -\infty, \quad \text{and} \quad F \to 0 \quad \text{as} \quad y \to +\infty.$$

If we temporarily think of F as a stream function then the boundary-value problem is the same as that for the irrotational flow parallel to a wall which contains a semi-infinite slot in the region $\{-L \leqslant x \leqslant L, y \geqslant 0\}$. The streamlines of such a flow are the contours of F. This latter problem is solved in a conventional way by using a conformal map of a uniform horizontal flow in the lower half of a complex w-plane. By application of the Schwartz–Christoffel theorem, the mapping from the w to the z-plane is

$$z = \frac{\pi}{2}\left\{(w^2-1)^{1/2} + \mathrm{i}\log\left[\frac{1-\mathrm{i}w-\mathrm{i}(w^2-1)^{1/2}}{1+\mathrm{i}w+\mathrm{i}(w^2-1)^{1/2}}\right]\right\}. \tag{3.15}$$

Let the real function $G(x, y)$ denote a harmonic complement of $F(x, y)$. We define the analytic function of position $\Phi = G + \mathrm{i}F$. The uniform flow, given by the complex potential $\Phi(w) = \frac{1}{2}\rho U_0 w\pi$, gives $w = 2\Phi/(\pi\rho U_0)$ and when substituted into (3.15) gives $z(\Phi)$. Now by holding F fixed, and varying G, (3.15) with $z = z(\Phi)$ becomes a parametric representation for the contours of F, in the z-plane. This expression is ideal for drawing contours: see figure 13(*a*). In the jet, $F = P_1$, so the contours of pressure impulse in the jet are the same as those drawn for F, but in $y < 0$ we must add the function $\rho U_0 y$ to F. This is done graphically in figure 13(*b*) by overlaying the lower half-plane of figure 13(*a*) with the straight contours of $\rho U_0 y$. The resultant Moiré pattern of intersections gives the contours of pressure impulse. The maximum pressure impulse is $0.247\rho U_0 L$. This should be compared with $0.742\rho U_0 L$ for jet impact on a rigid surface.

4. The velocity field and the splash

We now look at the velocity field after impact, $\boldsymbol{u}_a(\boldsymbol{x})$. For example consider the semi-infinite wave discussed in §3.1. From equations (2.2) and (3.1) and with $b = \infty$, the vertical component of velocity after impact is

$$v_a(x, y) = v_b(x, y) + U_0 \sum_{n=1}^{\infty} \frac{\cos\mu\lambda_n - 1}{\lambda_n} \cos(\lambda_n y/H) \exp(-\lambda_n x/H). \tag{4.1}$$

The velocity components are harmonic, so each takes its maximum value on the domain boundary. The most interesting velocity is at the free surface, and figure 14 shows the change in the vertical component as a function of distance from the wall. In the Appendix we show that near the origin $v_a(x, 0) \sim -(2U_0/\pi)\log(x/H)$ as x tends to 0. There is no singularity if the impact speed normal to the wall is chosen to decrease to 0 as $y \to 0$, or if the wall slopes backward from the free surface. See Okamura (1993) or consider the solution obtained by choosing any other pressure-impulse contour to represent the free surface. The high, or singular, velocity change at the boundary may give an indication of the strength of any splash.

The splash on impact of a liquid on a solid follows the rigid boundary whilst it is concave and may, or may not, follow a convex boundary. Despite some literature

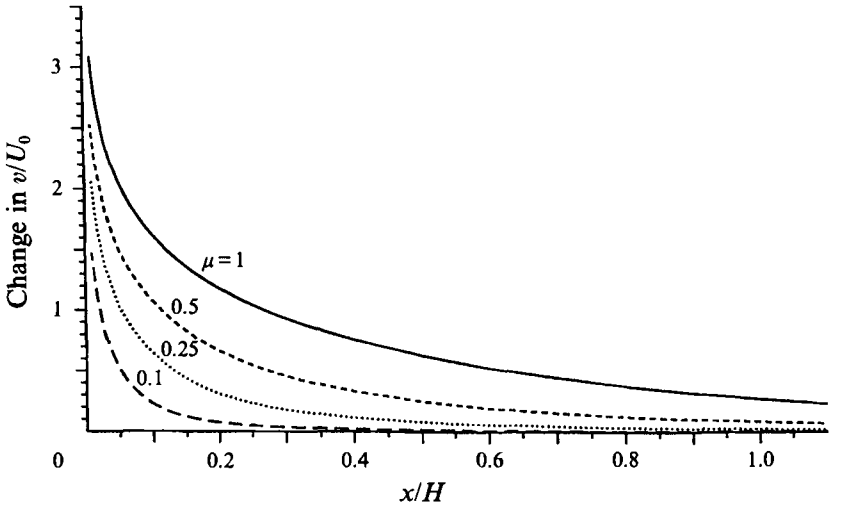

FIGURE 14. The change in the vertical velocity component at the free surface of a semi-infinite rectangular wave for several values of μ. The top of the wave is in uniform horizontal translation before impact so the curves indicate the free-surface shape soon after impact. The velocity is singular at $x = 0$ (see the Appendix).

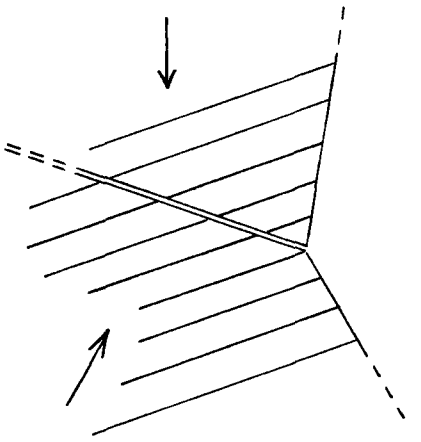

FIGURE 15. A simplified shape for the boundary of two impacting liquid bodies: two wedges with angles totalling more than 180° meeting on a common side.

searching we have failed to learn more about the convex rigid boundary than in Worthington's (1908) experiments which show dependence on both boundary roughness and splash velocity. At impact of two liquid regions there is no such obvious direction for the splash to go, and we here look at the information we can glean from the pressure-impulse model. This can only be expected to give the initial direction; more detailed knowledge is required for the evolution of the splash, e.g. see the thin-layer model of Peregrine (1981).

The example of §3.6 is such a liquid–liquid impact. The velocities at the edge of the impact area indicate that the initial splash direction bisects the angle between the two impacting surfaces. The device used to solve that problem can also be used to learn about the pressure impulse near the corner of two impacting free surfaces as shown in figure 15. The form of pressure impulse at impact near the corner can be found. There

is a singularity in gradient at the corner dominating the velocity field, provided the included angle in the liquid is greater than π. The direction of the gradient at the corner shows that the likely initial direction of splash is again along the bisector of the two free surfaces.

5. Energy dissipation

For the general pressure-impulse problem we show that the total kinetic energy decreases during impact. The change in gravitational potential energy is negligible because we suppose that the fluid does not move significantly during the impact.

Let V be the region occupied by the fluid at time t_b; then the impact brings about a change, ΔE_K, of kinetic energy given by

$$\Delta E_K = (E_K)_b - (E_K)_a = \int_V \tfrac{1}{2}\rho(\boldsymbol{u}_b^2 - \boldsymbol{u}_a^2)\,\mathrm{d}V. \tag{5.1}$$

From (2.2) we have $\boldsymbol{u}_a = \boldsymbol{u}_b - \nabla P/\rho$. Also P is harmonic, so we may express the integrand in (5.1) as a divergence:

$$\Delta E_K = \int_V \nabla\cdot\left\{P\left(\boldsymbol{u}_b - \frac{1}{2\rho}\nabla P\right)\right\}\mathrm{d}V. \tag{5.2}$$

Suppose the term between braces in (5.2) satisfies the following two conditions: (i) it has continuous first derivatives in V, and (ii) it tends to zero at infinity when V is an infinite domain. Then we can use the divergence theorem to reduce the integration to the boundary ∂V of V to obtain

$$\Delta E_K = \int_{\partial V} P\left(\boldsymbol{u}_b - \frac{1}{2\rho}\nabla P\right)\cdot\boldsymbol{n}\,\mathrm{d}S,$$

where $\boldsymbol{n}$ is the outward unit normal on ∂V and $\mathrm{d}S$ is an element of surface area of ∂V. Now $u_{nb} = \boldsymbol{u}_b\cdot\boldsymbol{n}$, so that

$$\Delta E_K = \left[\int_{\partial F} + \int_{\partial B} + \int_{\partial I}\right] P\left(u_{nb} - \frac{1}{2\rho}\frac{\partial P}{\partial n}\right)\mathrm{d}S. \tag{5.3}$$

In (5.3) ∂V has been re-expressed as the union of three disjoint sets: the free surface ∂F, the rigid boundary at which fluid stays in contact ∂B, and the impact zone ∂I. On ∂F, $P = 0$; on ∂B both u_{nb} and $\partial P/\partial n$ vanish; and on ∂I we have $\partial P/\partial n = \rho u_{nb}$. Also we suppose that u_{nb} is smooth enough to satisfy condition (i) above. Hence (5.3) simplifies to

$$\Delta E_K = \frac{1}{2}\int_{\partial I} P u_{nb}\,\mathrm{d}S. \tag{5.4}$$

For example, the kinetic energy loss per unit width of wall, for the semi-infinite rectangular wave discussed in §3.1, is

$$\Delta E_K = \rho H^2 U_0^2 \sum_{n=1}^{\infty} \frac{4}{\lambda_n^3}\sin^4(\tfrac{1}{2}\mu\lambda_n). \tag{5.5}$$

As a function of μ, ΔE_K has a maximum value, when $\mu = 1$, of $0.271\rho H^2 U_0^2$. This loss of energy on impact appears to have been discussed little before. It is noted by Zhang, Duncan & Chahine (1993) in their numerical modelling of jet impact in a collapsing

bubble, and is not surprising when the corresponding inelastic impact of a particle is considered. However, it is not immediately clear where the lost energy goes. Amongst neglected effects, compressibility comes to mind, but for low subsonic impacts the amount of energy available is very much greater than the sound waves ordinarily perceived.

Comparisons with cases like wedge entry (Howison *et al.* 1991) and the impact-like motions that can occur when waves meet walls ('flip-through' described in Cooker & Peregrine 1990*a*, *b*, 1995) are helpful. In these cases, there are 'outer' pressure fields corresponding to the pressure-impulse fields here, but the fluid flow is entirely irrotational and energy preserving. Energy is concentrated in the impact region forming narrow high-speed jets which we call splash. Similar high-speed jets are brought about by wavemakers moving into water initially at rest, such as the case of constant acceleration studied by King & Needham (1994).

Pressure-impulse theory does not pretend to describe the 'inner' region where the splash forms. It is tempting to equate the splash with the logarithmic singularity of the free surface velocity in equation (4.1): however, as noted, there is no singularity for a slightly different impact where energy loss still occurs. In the impact region, where neglected nonlinear terms are important and fluid displacements during impact are not small, this 'lost' energy accumulates and is associated with splash. It may be possible to extend the pressure-impulse theory to obtain measures of the width and velocity of the splash-forming jet, but we have yet to succeed. Detailed computations of this area are presented in work in the course of preparation.

6. Conclusion

The pressure-impulse approximation is used here to illustrate features of the pressure field due to wave impact on solid structures and related topics. By choosing relatively simple geometric shapes several features are demonstrated. In particular, the pressure-impulse field is insensitive to variations of the wave shape at distances greater than half the water depth from the impact region. This is useful for applications since it indicates that as long as the basic properties of the wave near impact can be estimated, most other details of wave shape are unimportant. The utility of the pressure-impulse approach is demonstrated in Cooker & Peregrine's (1992) discussion of the impulse on a body near the impact zone, where it is shown that the impulsive pressure gradient can be an important factor in moving armour units near a wall. Chan (1994) makes a comparison with experiments.

Where the impact occurs in a confined space the pressure impulse is increased. This increase has not been reported before, and merits further study, in application to the sloshing of liquids in containers and to the enhancement of pressures by cracks. Further work (Topliss 1994) reinforces the view that this increase can be significant.

Pressure-impulse calculations only give an integrated view of the pressure field. There is the obvious integration in time which occurs in definition (1.1) and the less easily defined approximation to the details of impact in the impact zone. Both of these should be fully appreciated if the most judicious use is to be made of pressure-impulse solutions.

The time integration of pressure, which gives the pressure impulse, is over the duration of a sharp pressure peak. Thus it can be reasonably estimated as if the time variation of the pressure has a sharp triangular peak of width Δt, an estimate of the peak pressure field is

$$p_{pk}(x) = 2P(x)/\Delta t. \tag{6.1}$$

As we have already indicated, there are much wider variations in p_{pk} than in P, which accords with a variation in Δt which is confirmed by experimental measurements. In practice Δt depends on details of the strongly nonlinear flow near impact and on any compressibility effects. Detailed numerical computations of flip through (Cooker & Peregrine 1990*a* and subsequent work) show a wide variation of timescales for nonlinear pressure peaks. Although there is no apparent lower limit of Δt, shorter times are clearly associated with smaller regions of 'impact' pressures.

Compressibility seems to be important in wave impacts only when air is trapped in the water. This air can be trapped as air pockets, or as dispersed bubbles. In either case free oscillation periods depend mainly on the volume of air trapped per unit length of the wall and the frequency of free oscillations gives a fair estimate of $1/\Delta t$. See Hattori, Arami & Yui (1994) for experiments, Peregrine (1994) for a discussion of dimensional and qualitative aspects and Topliss (1994) for further quantitative details. Useful guidelines for estimating Δt when there is trapped air should be obtainable from further experimental and theoretical analyses.

The most interesting result about the neglected details in the impact zone obtainable from a pressure-impulse calculation is the apparent loss of energy presented in § 5. For the case of a rigid body impacting liquid Korobkin (1994*a*, *b*) shows that half the energy goes into the splash and a quarter into compression. In the cases considered here, much of the energy must clearly go to the small-scale motion, but in a manner which probably depends strongly on the presence or absence of trapped air. The flip-through computations of Cooker & Peregrine (1995) are for incompressible irrotational flow, so no energy is lost. Thus the energy 'lost' in the pressure-impulse approximation must all appear in the jet going up the wall.

Financial support from the UK Science and Engineering Research Council research grants GR/F 28298 and GR/G 21032, and from the Commission of the European Communities, Directorate General for Science, Research and Development under MAST contract MAS2-CT92-0047, Monolithic Coastal Structures, is gratefully acknowledged.

Appendix. The pressure impulse for a semi-infinite rectangular wave expressed as an integral

In (3.1) let $b = \infty$, $X = -x/H$, $Y = y/H$, $U_0 = \rho = 1$. The sine and cosine terms of the series are re-written as complex exponentials:

$$P = \frac{1}{2\mathrm{i}} \sum_{n=1}^{\infty} \frac{1}{\lambda_n^2} \{e^{\lambda_n z_1} - e^{\lambda_n z_1^*} + e^{\lambda_n z_2} - e^{\lambda_n z_2^*} - 2e^{\lambda_n z_3} + 2e^{\lambda_n z_3^*}\}, \tag{A 1}$$

where $z_1 = X + \mathrm{i}(Y+\mu)$, $z_2 = X + \mathrm{i}(Y-\mu)$, $z_3 = X + \mathrm{i}Y$, where $*$ denotes complex conjugate, and $\lambda_n = (n-\frac{1}{2})\pi$. We split (A 1) into the sum of six separate series, each of the form

$$f(z) = \sum_{n=1}^{\infty} \frac{e^{\lambda_n z}}{\lambda_n^2}, \tag{A 2}$$

where z is any element of the set $\{z_1, z_1^*, z_2, z_2^*, z_3, z_3^*\}$. Now $\mathrm{Re}(z) < 0$. So we can differentiate the uniformly convergent series (A 2) twice with respect to z, giving a geometric series, which can be summed exactly to give $f''(z) = -\frac{1}{2}\mathrm{cosech}(\frac{1}{2}\pi z)$. Two

integrations give us an expression for $f(z)$ and this process leads to an integral representation of the summations in (A 1):

$$f(z) = \frac{1}{\pi}\int \log\{\operatorname{cosech}(\tfrac{1}{2}\pi z) + \coth(\tfrac{1}{2}\pi z)\}\,\mathrm{d}z, \tag{A 3}$$

and we define the analytic function

$$F(z) = f(z+\mathrm{i}\mu) + f(z-\mathrm{i}\mu) - 2f(z), \tag{A 4}$$

where $z = X+\mathrm{i}Y$. A restatement of (A 1) is now

$$P = \operatorname{Im}\{F(X+\mathrm{i}Y)\}. \tag{A 5}$$

The integral in definition (A 3) is indefinite, but there is no ambiguity in the subsequent definition of F (A 4), because the integration constant in (A 3) is self-cancelling in (A 4). At the wall, $X = 0$, (A 5) is

$$P(0, Y; \mu) = \operatorname{Im}\frac{1}{\pi}\int_Y^{Y+\mu} + \int_Y^{Y-\mu} \log(\operatorname{cosech}\tfrac{1}{2}\pi i s + \coth\tfrac{1}{2}\pi i s)\,\mathrm{i}\,\mathrm{d}s,$$

where s is real. This can be reduced to the following real integral:

$$P(0, Y; \mu) = \frac{1}{\pi}\int_Y^{Y+\mu} + \int_Y^{Y-\mu} \ln|\tan\tfrac{1}{4}\pi s|\,\mathrm{d}s. \tag{A 6}$$

The maximum value of P at the wall as a function of Y is given by $\partial P/\partial Y = 0$, i.e.

$$\log|\tan\tfrac{1}{4}\pi(Y+\mu)\tan\tfrac{1}{4}\pi(Y-\mu)| - 2\log|\tan\tfrac{1}{4}\pi Y| = 0.$$

After some manipulation the pressure-impulse maximum is found to be at $Y = Y_{max}$ where

$$\tan\tfrac{1}{4}\pi Y_{max} = -\left\{\frac{1-(1-\tan^4\tfrac{1}{4}\pi\mu)^{1/2}}{\tan^2\tfrac{1}{4}\pi\mu}\right\}^{1/2}, \quad \mu\in(0,1]. \tag{A 7}$$

From (A 7) we see that as $\mu\to 0$, $Y_{max} \sim -\mu/\sqrt{2}$. In fact this asymptotic relation is adequate for $\mu < 0.5$.

The singularity in the vertical velocity component v_a at $x = 0$, $y = 0$ is found as follows. Let $z = X+\mathrm{i}Y$, then from (A 5)

$$v_a = -\partial P/\partial Y = -\operatorname{Re}\{\mathrm{d}F/\mathrm{d}z\}.$$

From (A 3) and (A 5), on the free surface at $Y = 0$

$$\left.\frac{\mathrm{d}F}{\mathrm{d}z}\right|_{Y=0} = -\frac{1}{\pi}\log\left[\left\{\frac{\cosh^2\tfrac{1}{4}\pi X}{\sinh\tfrac{1}{2}\pi X}\right\}^2 \frac{\sinh\tfrac{1}{2}\pi(X+\mathrm{i}\mu)}{\cosh^2\tfrac{1}{4}\pi(X+\mathrm{i}\mu)}\frac{\sinh\tfrac{1}{2}\pi(X-\mathrm{i}\mu)}{\cosh^2\tfrac{1}{4}\pi(X-\mathrm{i}\mu)}\right]. \tag{A 8}$$

Hence

$$v_a \sim \frac{1}{\pi}\log\left\{\frac{16\tan^2(\tfrac{1}{4}\pi\mu)}{\pi^2 X^2}\right\} \quad \text{as} \quad X\to 0.$$

So we have the asymptotic result $v_a \sim -(2/\pi)\log X$ as $X\to 0$. Note that in dimensional units this result is $v_a \sim -(2/\pi)\,U_0\log[\pi x\cot(\mu\pi/4)/(4H)]$ as $x/H\to 0$.

REFERENCES

BAGNOLD, R. A. 1939 Interim report on wave pressure research. *J. Inst. Civil Engrs* **12**, 201–226.

BATCHELOR, G. K. 1973 *An Introduction to Fluid Dynamics*. Cambridge University Press.

BLACKMORE, P. A. & HEWSON, P. J. 1984 Experiments on full-scale wave impact pressures. *Coastal Engng* **8**, 331–346.

CHAN, E. S. 1994 Mechanics of deep water plunging-wave impacts on vertical structures. *Coastal Engng* **22**, 115–133.

CHAN, E. S. & MELVILLE, W. K. 1988 Deep water plunging wave pressures on a vertical plane wall. *Proc. R. Soc. Lond.* A **417**, 95–131.

COINTE, R. 1989 Two-dimensional water-solid impact. *Trans. ASME: J. Offshore Mech. Arctic Engng* **111**, 109–114.

COINTE, R. & ARMAND, J.-L. 1987 Hydrodynamic impact analysis of a cylinder. *Trans. ASME: J. Offshore Mech. Arctic Engng* **109**, 237–243.

COOKER, M. J. & PEREGRINE, D. H. 1990*a* Violent water motion at breaking wave impact. *Proc. 22nd Intl Conf. Coastal Engng, ASCE, Delft*, pp. 164–176. (Also *School of Mathematics, University of Bristol Rep.* AM-90-15.)

COOKER, M. J. & PEREGRINE, D. H. 1990*b* A model for breaking wave impact pressures. *Proc. 22nd Intl Conf. Coastal Engng, ASCE, Delft*, pp. 1473–1486.

COOKER, M. J. & PEREGRINE, D. H. 1992 Wave impact pressure and its effect upon bodies lying on the sea bed. *Coastal Engng* **18**, 205–229.

COOKER, M. J. & PEREGRINE, D. H. 1995 Computations of water wave impact and flip-through. In preparation.

CUMBERBATCH, E. 1960. The impact of a water wedge on a wall. *J. Fluid Mech.* **7**, 353–374.

DENNY, D. F. 1951 Further experiments on wave pressures. *J. Inst. Civil Engrs* **35**, 330–345.

FÜHRBÖTER, A. 1986 Model and prototype tests for wave impact and run-up on a uniform 1:4 slope. *Coastal Engng* **10**, 49–84.

GODA, Y. 1985 *Random Seas and the Design of Maritime Structures*. University of Tokyo.

HATTORI, M., ARAMI, A. & YUI, T. 1994 Wave impact pressure on vertical walls under breaking waves. *Coastal Engng* **22**, 79–114.

HOWISON, S. D., OCKENDON, J. R. & WILSON, S. K. 1991 A note on incompressible water entry problems at small dead-rise angles. *J. Fluid Mech.* **222**, 215–230.

HWANG, J.-B. G. & HAMMITT, F. G. 1977 High-speed impact between curved liquid surface and rigid flat surface. *Trans. ASME: J. Fluids Engng* **99**, 396–404.

JOHNSTONE, E. A. & MACKIE, A. G. 1973 The use of Lagrangian coordinates in the water entry and related problems. *Proc. Camb. Phil. Soc.* **74**, 529–538.

JOLLEY, J. G. W. 1961 *Summation of Series*. Dover.

KING, A. & NEEDHAM, D. J. 1994 The initial development of a jet caused by fluid, body and free surface interaction. *J. Fluid Mech.* **268**, 89–101.

KIRKGÖZ, M. S. 1982 Shock pressure of breaking waves on vertical walls. *J. Waterways, Port Ocean Engng Div. ASCE* **108**, 81–95.

KIRKGÖZ, M. S. 1991 Impact pressure of breaking waves on vertical and sloping walls. *Ocean Engng* **18**, 45–59.

KOROBKIN, A. 1992 Blunt body impact on a compressible liquid surface. *J. Fluid Mech.* **244**, 437–453.

KOROBKIN, A. 1994*a* Blunt-body penetration into a slightly compressible liquid. *20th Symposium on Naval Hydrodynamics*.

KOROBKIN, A. 1994*b* Some integral characteristics in the jet impact problem. *J. Fluid Mech.* (submitted).

KOROBKIN, A. & PUKHNACHOV, V. V. 1988 Initial stage of water impact. *Ann. Rev. Fluid Mech.* **20**, 159–185.

LAMB, H. 1932 *Hydrodynamics*, 6th Edn. Cambridge University Press.

LESSER, M. B. 1981 Analytic solutions of liquid drop impact problems. *Proc. R. Soc. Lond.* A **377**, 289–308.

LESSER, M. B. & FIELD, J. E. 1983 The impact of compressible liquids. *Ann. Rev. Fluid Mech.* **15**, 97–122.

MILNE-THOMSON, L. M. 1968 *Theoretical Hydrodynamics*, 5th Edn, Examples xvii, prob. 44, p. 544. Macmillan.

NAGAI, S. 1960 Shock pressures exerted by breaking waves on breakwaters. *J. Waterways, Harbors Div. ASCE* **86**, 1–38.

OKAMURA, M. 1993 The impulsive pressure due to wave impact on an inclined plane wall. *Fluid Dyns Res.* **12**, 215–228.

PARTENSCKY, H. W. & TOUNSI, K. 1989 Theoretical analysis of shock pressures caused by waves breaking at vertical structures. *Proc. XXIII Congr. IAHR, Ottawa* (ed. J. Ploeg), vol. C-113–118.

PEREGRINE, D. H. 1981 The fascination of fluid mechanics. *J. Fluid Mech.* **106**, 59–80.

PEREGRINE, D. H. 1994 Pressure on breakwaters: a forward look. *Intl Workshop on Wave Barriers in Deep Waters, Port and Harbour Research Institute, Japan* (ed. T. Takayama), pp. 553–573.

RICHERT, G. 1968 Experimental investigation of shock pressures against breakwaters. *Proc. 11th Conf. Coastal Engng, ASCE*, pp. 954–973.

ROBERTS, A. 1987 Transient free surface flows generated by a moving vertical plate. *Q. J. Mech. Appl. Maths* **40**, 128–158.

ROUVILLE, A. DE, BESSON, P. & PETRY, P. 1938 Etat actuel des études internationales sur les efforts dus aux lames. *Ann. Ponts Chaussées* **108**, 5–113.

SAVIC, P. & BOULT, G. T. 1957 The fluid flow associated with the impact of liquid drops with solid surfaces. *Heat Transfer and Fluid Mechanics Inst., Cal. Tech.*, pp. 43–84.

SEDOV, L. I. 1965 *Two-Dimensional Problems in Hydrodynamics and Aerodynamics* (transl. from Russian by C. Chu, H. Cohen, B. Seckler). Wiley Interscience.

STEVENSON, T. 1886 *Design and Construction of Harbours*, 3rd Edn. Black.

TOPLISS, M. E. 1994 Water wave impact on structures. Ph.D. dissertation, University of Bristol.

WAGNER, H. 1932 Uber Stoss- und Gleitvorgange an der Oberfache. *Z. Angew. Math. Mech.* **12**, 193–215. (English transl: Phenomena associated with impacts and sliding on liquid surfaces. *NACA Translation* 1366.)

WEGGEL, J. R. & MAXWELL, W. H. C. 1970 Numerical model for wave pressure distributions. *J. Waterways Harbours, Coastal Engng Div. ASCE* **96**, 623–642.

WIJNGAARDEN, L. VAN 1980 Sound and shock waves in bubble liquids. In *Cavitation and Inhomogeneities in Underwater Acoustics* (ed. W. Lauterborn), pp. 127–140. Springer.

WITTE, H.-H. 1988 Druckschlagbelastung durch Wellen in deterministischer under stochastischer Betrachtung. *Mitteilungen, Leichtweiss Inst. für Wasserbau, Tech. University Braunschweig*, vol. 102, pp. 1–227.

WORTHINGTON, A. M. 1908 *A Study of Splashes*. Longmans Green & Co. (see also 1963 reprint, Macmillan).

ZHANG, S., DUNCAN, J. H. & CHAHINE, G. L. 1993 The final stage of the collapse of a cavitation bubble near a rigid wall. *J. Fluid Mech.* **257**, 147–181.